Accepted Manuscript

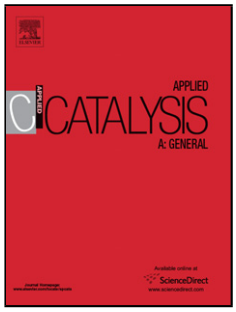

Title: Preferential oxidation of CO in excess of H_2 on Pt/CeO_2-Nb_2O_5 catalysts

Author: E.O. Jardim S. Rico-Francés F. Coloma J.A. Anderson Enrique V. Ramos-Fernandez J. Silvestre-Albero A. Sepúlveda-Escribano

PII: S0926-860X(14)00794-7
DOI: http://dx.doi.org/doi:10.1016/j.apcata.2014.12.032
Reference: APCATA 15171

To appear in: *Applied Catalysis A: General*

Received date: 26-6-2014
Revised date: 26-11-2014
Accepted date: 15-12-2014

Please cite this article as: E.O. Jardim, S. Rico-Francés, F. Coloma, J.A. Anderson, E.V.R.-F. </sup>,J. Silvestre-Albero, A. Sepúlveda-Escribano, Preferential oxidation of CO in excess of H_2 on Pt/CeO_2-Nb_2O_5 catalysts, *Applied Catalysis A, General* (2014), http://dx.doi.org/10.1016/j.apcata.2014.12.032

- Pt catalysts supported on CeO_2-Nb_2O_5 mixed oxides were studied
- **The formation of solid solution was demonstrated**
- Mixed oxides behave better than pure oxides.
- Optimal catalyst composition was found

Preferential oxidation of CO in excess of H_2 on Pt/CeO_2-Nb_2O_5 catalysts

E.O. Jardim[1], S. Rico-Francés[1], F. Coloma[1], J. A. Anderson [2], Enrique V. Ramos-Fernandez[1],J. Silvestre-Albero[1] and A. Sepúlveda-Escribano[1].*

[1]Laboratorio de Materiales Avanzados, Departamento de Química Inorgánica – Instituto Universitario de Materiales de Alicante. Universidad de Alicante, Apartado 99, E-03080 Alicante, Spain.

[2]Surface Chemistry and Catalysis Group, Department of Chemistry, University of Aberdeen, AB24 3UE Scotland (UK).

*Corresponding author:

e-mail:enrique.ramos@ua.es

Abstract

A series of CeO_2-Nb_2O_5 mixed oxides with different Nb content, as well as the pure oxides, have been synthesized by co-precipitation with excess urea. These materials have been used as supports for platinum catalysts, with $[Pt(NH_3)_4](NO_3)_2$as precursor. Both supports and catalysts have been characterized by several techniques: N_2 physisorption at 77 K, X-ray diffraction, Raman spectroscopy, X-ray photoelectron spectroscopy, UV-Vis spectroscopy, scanning electron microscopy, transmission electron microscopy, temperature-programed reduction and temperature-programmed desorption (CO and H_2),and their catalytic behavior has been determined in the PROX reaction, both with an ideal gas mixture (CO, O_2 and H_2) and insimulated reformate gas containing CO_2 and H_2O. Raman spectroscopy analysis have shown the likely substitution of some Ce^{4+}cations by Nb^{5+} to some extent in supports with low niobium contents. Moreover, the presence of Nb in the supports hinders their ability to adsorb CO and to oxidize it to CO_2. However, an improvement of the catalytic activity for CO oxidation is obtained by adding Nb to the support, although the Pt/Nb_2O_5catalyst shows very low activity. The best results are found with the $Pt/0.7CeO_2$-$0.3Nb_2O_5$catalyst, which shows a high CO conversion (85 %) and a high yield (around 0.6) after a reduction treatment at 523 K. The effect of the presence of CO_2 and H_2O in the feed has also been determined.

Keywords: Platinum, niobia, ceria, DRIFT, PROX.

1. Introduction

One of the most interesting aspects of ceria-based catalysts is that their properties strongly depend on the pre-treatment conditions used and on the exact composition of the oxide. In this sense, it is known that the oxygen storage capacity (OSC) of pure ceria is inhibited when it is used in high temperature applications, e.g. automotive applications.However, it can be thermally stabilized, for example, by incorporation of a second cation such as Zr[1]. The large number of applicationsof ceria-based catalystslie on properties such as (i) the crystal size, that canbe tailored by modifying the synthesis conditions[2]; (ii) its reducibility, that can be altered by incorporationof other metals (e.g., Ce-Zr) due to the formation of a solid solution[1]; (iii) the present of defect sites, which modifies this reducibility[3], and (iv) the ability of cerium to easily change between the Ce^{3+} and Ce^{4+} states. It is also known that the ionic conductivity of ceria is enhanced by doping with other rare-earth cations. Moreover, these effects depend on the ionic radius of the doping cation[4], and its ability to distort the ceria lattice structure[5]. O'Connell *et al*.[6]suggested that the anion vacancies produced by the introduction of M^{3+}ions into the ceria lattice may enhance its catalytic behavior. It is known that doping with other ions could enhancethe activity for different reasons. For example, in the case of M^{5+} ions asniobium, the introduction of extra oxygen anions that would be more easily removed is expected[7].

Niobium-based materials are effective catalysts in several applications, such as pollution abatement[8], selective oxidation[9],epoxidation[10],hydrocarbon conversion reactions[7], hydrogenation and dehydrogenation[11], photochemistry and electrochemistry [12] among others. The number of references in the literature concerning niobium catalysts has been steadily increasing over the last two decades, which reflects the growing interest in this area of research.A major application of niobium-based catalysts has been in the area of oxidation reactions, due to the redox properties of niobium oxide catalysts. Niobia-doped ceria materials have shown agood tolerance to carbon deposition [9] and excellentproperties as solid oxide fuel cell (SOFC) anodes[12]. However, more research is necessary in order to extent the improved performance of these systems for other applications[12]. For example the excellent electrical properties of niobia-doped ceria were already reported by Naik and Tien [13] and De Guire*et al*.[14]. Some authors have also studied niobia-based catalysts

for the CO oxidation reaction. Guerrero *et al.*[15]studied the promoting effect of alumina-supported niobia in the PROX reaction. The results showed that at low niobia loading, the catalysts exhibited an increase in the CO oxidation activity and selectivity. On the contrary, Marques *et al*. [16]showed a low selectivity for Pt-Sn/Nb_2O_5 or Pt/Nb_2O_5 catalysts in the CO oxidation reaction in the presence of H_2,which could be explained in terms of platinum modification by niobia (strong metal-support interaction effect - SMSI) and thepresence tin (bimetallic effect).

The aim of this work has been to study the catalytic activity of platinum supported on ceria-niobia mixed oxides of different composition in the preferential CO oxidation in the presence of H_2 (PROX). The physico-chemical properties of supports and catalysts have been evaluated by a number of techniques, in an attempt to correlate them with the observed catalytic behavior.

2. Experimental

2.1. Catalystspreparation

A series of niobia-ceria supports were prepared by the urea precipitation method. The appropriate amounts of $Ce(NO_3)_3 \cdot 9H_2O$ (Aldrich, 99 %) and ammonium niobate (V) oxalate hydrate (Aldrich, 99.99 %) to obtain different $xCeO_2$-(1-x)Nb_2O_5 supports with x = 1, 0.9, 0.7, 0.4 and 0, together with excess urea (Fluka, 98 %), were dissolved in 400 ml of ultra-pure water. The solutions were heated at 363 K to induce urea hydrolysis, with constant stirring for 11 h. Finally, ammonia solution was added drop-wise to ensure complete precipitation. The solids were separated by filtration, washed with ultra-pure water, and dried overnight at 383 K. Finally, they were calcined in air at 773 K for 4 h, with a heating rate of 3 $K \cdot min^{-1}$.Pt/$xCeO_2$-(1-x)Nb_2O_5 catalysts were prepared by incipientwetness impregnation method. The supports were impregnated with an aqueous solution of $[Pt(NH_3)_4](NO_3)_2$(Aldrich, 99.9 %), in the appropriate amount to achieve a 1 wt.% Pt loading. Finally, the catalysts were dried at 383 K overnight, and calcined in air at 773 K for 2 h, witha heating rate of 3 $K \cdot min^{-1}$.

2.2. Catalysts characterization

The textural properties of the supports were characterized by N_2 adsorption measurements at 77 K. Gas adsorption experiments were performed in ahome-developed fully automated manometricapparatus. Prior to the adsorption experiments,

samples were out-gassed under vacuum (10^{-4} Pa) at 523 K for 4 h. The *"apparent"* surface area was estimated after application of the BET equation.

The actual metal loading of the different catalysts was determined by ICP in a Perkin–Elmer device (Optimal 3000). To this end, the metal was extracted from the catalysts by refluxing them in aqua regia for 8 h.

X-ray fluorescence (XRF)analyses wereobtained on a X-ray sequential spectrometer PHILIPS MAGIX PRO equipped with a rhodium X-ray tube and a beryllium window.

X-ray powder diffraction patterns were recorded on a Bruker D8-Advance system with Göebel mirror and a Kristalloflex K 760-80F X-ray generation, fitted with a Cu cathode and a Ni filter. Spectra were registered between 20 and 80º (2θ) with a step of 0.05 º and a time per step of 3s.

TEM images were obtained on a JEOL electron microscope (model JEM-2010) working at 200 kV. It was equipped with an INCA Energy TEM 100 analytical system and a SIS MegaView II camera. Samples for analysis were suspended in ethanol and placed on copper grids with a holey-carbon film support.

SEMmicrographs were obtainedon a scanning electron microscope Hitachi S3000N, which is equipped with a Bruker XFlash 3001 X-ray detector for microanalysis (EDS) and mapping.

Raman spectra were recorded on a FT-Raman Bruker RFS/100 spectrometer with coupled microscope. Spectra were recorded at room temperature (274 K, 85 % relative humidity) between 4000 and 400 cm^{-1} with a spectral resolution of 4 cm^{-1}. Raman spectra were obtained using different conditions depending on the type of sample used. In the case of samples with a very intense Raman effect, a laser power of 100mW and 32 scans was used, whereas for other samples (for example, those with a larger amount of niobium) 200 mW were used and between 128 to 256 scans collected. Calibration was carried out with a silicon single crystal at 520.7 ± 2 cm^{-1}.

Temperature-programmed reduction (TPR) with H_2 measurementswere carried out oncalcined catalysts in a U-shaped quartz cell using a 5% H_2/He gas flow of 50 $mL \cdot min^{-1}$, with a heating rate of 10 $K \cdot min^{-1}$. Samples were treated with flowing He at 423 K for 1 h before the TPR run. Hydrogen consumption was followed by on-line mass spectrometry.

Temperature-programmed CO desorption experiments on supports and reduced catalysts were carried out in a U-shaped quartz cell using 10 %CO/He at50 $mL \cdot min^{-1}$.

Samples were first reduced with flowing H_2 at 523 K (5 K·min^{-1}) for 1 h and then cooled to room temperature in He flow (50 mL·min^{-1}) to remove hydrogen from the catalyst's surface. Then, the samples were exposed to the CO/He flow for 1 h. Physisorbed CO was removed by purging with He at room temperature. CO desorption was performed in He flow up to 773 K, with a heating rate of 10 K·min^{-1}, and monitored by on-line mass spectrometry.

Temperature-programmed desorption of H_2 was carried out on supports and catalysts in a U-shaped quartz cell using a 10% H_2/He gas stream (50 mL·min^{-1}). Samples were reduced with flowing H_2 at 523 K (5 K·min^{-1}) for 1 h and then cooled to room temperature in flowing He (50 mL·min^{-1}). Then, samples were exposed to the H_2/He flow for 1 h. Weakly adsorbed H_2 was removed by purging with He, and then H_2 desorption was performed in flowing He by heating at 10 K·min^{-1} up to 773 K. Hydrogen evolution was monitored by on-line mass spectroscopy.

X-Ray photoelectron spectroscopy (XPS) analyses were performed with a VG-MicrotechMultilab 3000 spectrometer equipped with a hemispherical electron analyzer and a Mg-K_α (h=1253.6 eV; 1 eV = 1.6302×10^{-19} J) 300-W X-ray source. The powder samples were pressed into small Inox cylinders, mounted on a sample rod placed in a pre-treatment chamber, and reduced in flowing H_2 for 1 h at 523 or 773 K before being transferred to the analysis chamber. Before recording the spectra, the samples were maintained in the analysis chamber until a residual pressure of ca. 5×10^{-7} N·m^{-2}was reached. The spectra were collected at pass energy of 50 eV. The intensities were estimated by calculating the integral of each peak, after subtracting the S-shaped background, and by fitting the experimental curve to a combination of Lorentzian (30%) and Gaussian (70%) lines. All binding energies were referenced to the C 1s line at 284.6 eV, which provided binding energy values with an accuracy of ±0.2 eV.

2.2. Catalytic behavior

The activity of the catalysts in the PROX reaction was determined in the temperature range 313to473 K at atmospheric pressure, with a reaction mixture (50 mL·min^{-1}) containing 20%H_2, 2%CO, 0.6-2%O_2,0-5 %CO_2, 0-5 %$H_2O$and He as balance (GHSV = 17000 h^{-1}). Before any catalytic measurement, catalysts were reduced *in situ*at 523 K or 773 K for 1 h under flowing H_2 (50 mL·min^{-1}).Reaction products were analyzed by on-line gas chromatography (TCD and FID), using a Plot/Q and a

Molesieve capillary column to separate the reactants and the reaction products. Only CO_2 and H_2O were detected as products.

Diffuse reflectance infrared Fourier transform spectroscopy (DRIFTS) *in situ* analysis was used to evaluate the adsorbed species present on the catalysts under reaction conditions. DRIFT spectra were collected using a Perkin-Elmer 100 FTIR fitted with a MCT detector. On-line gas analysis was performed using a BaltzersPrismaQuadrupole mass spectrometer. The DRIFTS cell (Harrick DRP-series) was fitted with ZnSe windows.Before exposure to the reactant mixture, samples were reduced *in situ* under flowing hydrogen (40 $mL \cdot min^{-1}$) at 523 K for 1 h, at a heating rate of 5 $K \cdot min^{-1}$. DRIFT spectra were recorded at 4 cm^{-1} resolution as an average of 10 scans. The gas mixtures were prepared using a computer-controlled gas-blender (Signal) with 40 $mL \cdot min^{-1}$ passing through the catalyst bed which equates to a GHSV = 17000 h^{-1} using about 100 mg of sample.CO oxidation was studied between 313 and 473 K, with a reactant mixture containing 20%H_2, 2%CO, 10% air and N_2 as a balance.

The CO conversion (X_{CO}), the selectivity towards CO_2 (S_{CO2}), as well as the yield to CO_2 and the λ value, were calculated using the following equations:

$$X_{CO} = 100 \cdot ([CO]_{in} - [CO]_{out})/[CO]_{in}$$

$$S_{CO2} = 100 \cdot 0.5 \cdot ([CO]_{in} - [CO]_{out})/([O_2]_{in} - [O_2]_{out})$$

$$CO_2 Yield = X_{CO}/100 \cdot S_{CO2}/100$$

$$\lambda = 2 \cdot [O_2]/[CO]$$

3. Results and discussion

3.1. Catalystscharacterization

Table 1reports the chemical composition of the prepared catalysts and their BET surface areas.It can be seen that the composition of the oxides covers a wide range, from pure ceria to pure niobia. Samples will be labelled with the nominal composition, which in all cases differs only slightly from the actual values.It can be seen that the addition of niobium to ceria gradually increases the surface areas of the supports, from 70 $m^2 \cdot g^{-1}$

for pure ceria to 132 m^2/g for pure niobia.This increase of the surface area could be explained on the basis of the incorporation of niobium into the ceria lattice, this yielding a mixed oxide with modified crystallinity, but it can also be due to a promoting effect of niobia hindering the formation of large ceria nanocrystals.Similar behavior has been described in the literature. Guerrero *et al*.[15]prepared Nb-Al_2O_3 supports with different niobia content by co-precipitation of ammonium niobium oxalate and colloidal alumina sol with excess aqueous ammonia, and the solids calcined at 500 ºC. They observed that the BET surface area increased with Nb loading up to 20% and the decreased at higher loadings.Regarding CeO_2-Nb_2O_5 systems, Stosic*et al.* observed a similar trend, i.e., addition of a small amount of niobia (25 wt.%) at first increased the surface areas, but they decreased with a further increase of the niobia content (75 wt.%).It worths to mention that the Stosic's method differs from our method in the precipitation procedure and in the calcination temperature; this can explain the slightly different results we have obtained[17].

The XRD patternsof Pt/xCeO_2-(1-x)Nb_2O_5catalysts are presented in Fig. 1. They show the six main diffraction lines of the fluorite structure of ceria [18] (face centred cubic structure). Addition of niobia produces both a progressive decrease in the peak intensity and the broadening of the main diffraction peaks, this indicating a decrease in crystallinity and/or a decrease in crystal size, in close agreement with the textural properties described before. Furthermore, additional peaks attributed to the hexagonal structure of niobium oxide were only observed in catalysts with high niobium contents (Pt/0.4CeO_2-0.6Nb_2O_5 and Pt/Nb_2O_5 catalyst) [19]. No diffraction peaks characteristic of Pt phases could be identified (Fig. 1), due to the low Pt loading and/or to the small Pt crystal sizes, below the XRD sensitivity. The metal particle size distribution could not be calculated from TEM images (not shown) because of the high metal dispersion (very small Pt nanoparticles). However, the presence of Pt was confirmed by EDS.

The average ceria crystallite sizes calculated by application of the Scherrer's equation are listed in Table 1. A gradual decrease in the ceria crystal size (from 17 to 6 nm) with increasing niobia content is clearly observed. This decrease in crystallinity would indicate that Nb hinders the formation of larger ceria particles by incorporation in the lattice. It produces a lattice distortion and, consequently, the ceria crystal growth is suppressed[20] .

Data in Table 1 show that there is no modification of the lattice constant with increasing in the niobia content, based on the (111) plane and considering the ceria

cubic phase. This observation could indicate that niobium cations may not be substituting for cerium cations in the fluorite-type structure [21], even though no separate niobium oxide phases could be detected. This may be due to the amorphous character of the niobia phase formed. However, the incorporation of Nb^{5+} in the lattice must not be discarded.

Raman spectroscopy measurements were carried out on the supports in order to further analyze the possible formation of a solid solution and to confirm the phases present in each sample (Fig. 2). The spectrum of pure niobia shows a broad band at 714 cm^{-1}, which is typical for all niobium oxides and is assigned to the vibrations of Nb-O-Nb bridges from slightly distorted octahedral NbO_6 connected with sharing corners [17, 22]. The Raman spectrum of pure ceria exhibits a main peak at 462.9 cm^{-1}, which is assigned to F_{2g} mode due to symmetrical stretching of Ce-O vibrational unit in eightfold coordination[23-25]. It is interesting to note the decrease of the intensity of this band with an increase of the niobia content. This can be due to the deformation of the framework after niobium incorporation or due to the ceria crystal size. Furthermore, this decrease is accompanied by a shift of this peak to 463.9 cm^{-1} for supports with x = 0.9 and x = 0.7, although no shift was observed for the support with x = 0.4.

It has been extensively reported that the peak at 462.9 cm^{-1} is shifted to progressively lower energies as the crystal size gets smaller, and the peak gets progressively broader. In our case, the crystal size strongly decreases with Nb content (as XRD results shows). However, the Raman mode at 462.9 cm^{-1} does not shift to lower energies, but to higher ones [26]. This shift is attributed to the lattice distortion due to the incorporation of a smaller cation, such as Nb^{5+}. It can then be concluded that the substitution of some Ce^{4+}cations by $Nb5^{+}$ takes place in supports with low niobia contents.

On the other hand, the characteristic band of niobia only appears in the spectrum of the support with a high niobium content, x = 0.4, and it is centered at 706 cm^{-1}.This shift with regards to pure niobia (714 cm^{-1}) can indicate that in this sample, some Nb^{5+}cations are being replaced with Ce^{4+}, this distorting its structure to some extent. A separated ceria phase is still present, as shown by XRD (Fig. 1).

Chemical mapping was used to analyze the distribution of cerium and niobium on the surface of the catalysts. Fig. 3a shows the SEM micrographs for catalysts $Pt/0.9CeO_2$-$0.1Nb_2O_5$, $Pt/0.7CeO_2$-$0.3Nb_2O_5$ and $Pt/0.4CeO_2$-$0.6Nb_2O_5$. It is interesting

to observe the different morphology of the catalysts as a function of the niobia content, shifting towards thin, needle-shaped particles. It is also worthwhile highlighting the decrease in the particle size after niobium incorporation, in close agreement with the textural properties described above.

From the SEM-chemical mapping analysis of cerium and niobium (Fig.3b and c, respectively) it is possible to observe the good distribution of both metals in two of the catalysts evaluated (x = 0.9 and x = 0.7 catalysts). However, in the case of x = 0.4 areas richer in Nb_2O_5 can be observed and that high niobia concentrations (rich areas) are presented as agglomerated particles. This confirms the results obtained by XRD and Raman, where the presence of two segregated oxide phases in the support containing high niobia content exists.

The H_2-TPR profiles for the $xCeO_2$-(1-x)Nb_2O_5supports and$Pt/xCeO_2$-(1-x)Nb_2O_5catalysts, x = 1, 0.9, 0.7, 0.4 and 0, are shown in Fig.4(a) and (b), respectively, which showthe rate of H_2 consumption as a function of temperature.The reduction of ceria (Fig. 4a) takes place in two regions, the first one centered at 760 K and the second one at 1050 K, which are assigned to the surface reduction and bulk reduction, respectively[27-31].Identical redox profiles to those of pure ceria were obtained for supports with low niobium content. However, incorporation of niobium gives rise to a decrease in the amount of ceria reduced at high temperature (bulk reduction) together with a slight increase in the hydrogen consumption at low temperature, and this could be related to the smaller ceria particle size. On the other hand, the H_2-TPR profile of the pure niobia support shows reduction at a much higher temperature(*ca.*1170 K). This peak is also present in the profile of the support with x = 4.

Incorporation of Pt to these supports facilitates ceria reduction, as shown in Fig. 4b.The H_2-TPR profile of Pt/CeO_2 (x = 1) shows two overlapping peaks due to hydrogen consumption at 575 and 610 K, which are assigned to the reduction of oxidized platinum species as well as surface ceria in close interaction with the metal, respectively. This is further confirmed by the quantification of the H_2 consumed (777 μmol/(g_{cat})), which is ~15 times higher than thatneeded for the complete reduction of the platinum precursor (51 μmol/(g_{cat})). These temperatures are higher than those found in other studies, where they are centered at around 400 K[32, 33],and may be a consequence of the higher temperature of the thermal treatment at which the catalyst has been submitted after preparation (calcination in air at 773 K), thatgenerates oxidized platinum species with a greater interaction with the ceria support. Catalysts

containingniobiaare all reduced at 350 – 375 K, which includes reduction of oxidized platinum species together with the surface reduction of ceria in the support[34]. The incorporation of Nb in the fluorite structure produces a big shifting in the temperature of reduction, this indicating an important effect on the reducibility of the catalysts. Hydrogen consumption in the TPR experiments does not follow a clear trend, since in samples with low cerium content (x=0.4) we also detected a niobium-based phase together with the ceria fluorite structure substituted with Nbcations.

Thereduction peak at ~400 K is very small in the catalyst supported on pure niobiaconfirming that, in this case, no surface reduction of the support takes place. When we quantified the H_2 consumption for this peak (~55 μmol/g) we found out that fits the hydrogen needed to reduce Pt oxide to metallic platinum (51 μmol/g).

Itis apparent from these TPR results that in all the catalysts supported on mixed oxides the reduction treatment at 523 K is enough to produce surface ceria reduction. This reduction temperature will be used later on in this study.Only in the cases of catalysts supported on pure ceria and pure niobiathe reduction treatment at this temperatureseems insufficient to produce any surface modification.

The chemical state of surface elements and their concentration in the $Pt/xCeO_2$-$(1-x)Nb_2O_5$catalysts after calcination at 773 K was evaluated by XPS. The binding energies of photoelectron peaks corresponding to the O 1s level are reported in Table 2 (Supporting information SI1). The experimental band can be deconvoluted into ~~two~~ three contributions, the lowest binding energy peak being ascribed to lattice oxygen species (O^{2-}) [35-38], whereas the peak at intermediates binding energies is assigned to less electron-rich oxygen species. Studies described in the literature have assigned the bands appearing at intermediates~~,~~ O_2^{2-}/O^{1-}[38, 39], or related to hydroxyl species, -OH[40] and probably also from carbonate species, CO_3^{2-}[41] (the C 1s spectra also showed a small component at 289.0 eV). All these species have been deconvoluted in a single peak, since the difference in binding energies is very small and all these species are prompt to participate in the reaction. Finally, the component at the highest binding energies is assigned to adsorbed molecular water [40, 42]

From results in Table 2, a displacement of the O 1s bands to higher binding energies with the increase of the niobium content can be observed. This suggests that more covalent metal–oxygen bonds are established, with less electron rich oxygen species [43]. These results are in agreement with the Raman spectra, where the peak at 462 cm^{-1} is shifted due to the niobium incorporation in the lattice.

In terms ofNb/Ce atomic ratio, the catalysts with less niobia content show values seven times higher than the bulk atomic ratio (Table 2). This behavior can be explained on the basis of a higher surface content of niobium oxide. It is well reported that the dopant tends to segregate towards the surface during the calcination and reduction treatments[44, 45].

The substitution of Nb^{5+} by Ce^{4+} in the niobium oxide network adds a negativecharge which may make up for an oxygen vacancy trapping one electron. However, the substitution of Ce^{4+} by Nb^{5+} in the ceria network brings a positive charge which may be compensated by the formation of Ce^{3+} ions. Zhang *et al*. [46]showed the increase of Ce^{3+}concentration in a double layer CeO_2/Nb_2O_5 thin film. It has been justified that the diffusionof Nb^{5+} from the CeO_2/Nb_2O_5 interface takes place following this reaction, Equation 1:

$$Ce^{4+}O_2 + xNb_2^{5+}O_5 \rightarrow Ce_{1-2x}^{4+}Ce_{2x}^{3+}Nb_{2x}^{5+}O_{2+4x} + \frac{x}{2}O_2 \quad \text{(Eq.1)}$$

In this case, the Nb^{5+}ion diffuses into the CeO_2 thin film to replace Ce^{4+}. The same amount of Ce^{4+}in CeO_2 films will be reduced to Ce^{3+}due to the neutrality, whereas the concentration of Ce^{3+}ion in the CeO_2/Nb_2O_5 thin film will be increased compared with the CeO_2 thin film.

The XPS analysis of the Pt $4f_{7/2}$ level indicates that, in practically all catalysts, platinum reduction after hydrogen treatment at 523K was complete (binding energies at around 71.0 eV). Only in Pt/CeO_2 and $Pt/0.9CeO_2$-$0.1Nb_2O_5$ catalysts, the metal was incompletely reduced (45% and 28% respectively) after this low temperature reduction treatment. The Pt/(Nb+Ce)atomic surface ratiosin the fresh calcined samples were 0.006, 0.03, 0.016, 0.014 and 0.008 for the catalyst series (x= 1, 0.9, 0.7, 0.4 and 0, respectively). This trend is maintained after the reduction treatments in hydrogen at 523 and 723K, without significant modifications in the values. Curiously, the highest platinum dispersion (as obtained from XPS analysis) occurs in the catalyst with the lowest surface area.

At thispoint, thecharacterizationresultssuggestthat Nb incorporation in thecerialatticeisfavored, and a solidsolutionwasformedforlow Nb concentrations. Anotherimportant factor istheredoxproperties of thecatalysts. Toanalysethispoint$Pt/xCeO_2$-$(1-x)Nb_2O_5$ catalysts was also characterized by

temperature-programmed desorption experiments from samples previously saturated with CO. It is worth noting that some of the CO adsorbed is desorbed as CO_2(Fig 7a).The presence of niobium in the support appears to hinder the formation of CO_2 at low temperature. This may be related to a decrease of oxygen mobility of the support in the presence of niobium. However, it is interesting to add that all catalysts doped with niobium showed less CO_2 formation than Pt/CeO_2. The niobium-containing catalysts showed a high CO conversion at low temperatures, as will be shown below; it looks counterintuitive since what a catalyst that oxidizes CO at low temperature is desired. It is important to bear in mind that the lattice oxygen carries out the oxidation of CO in the TPD experiment generating vacancies. In the catalytic experiment these vacancies need to be regenerated, and this is a different process that can at different speed and at different temperature.

The CO desorption profiles are shown in Fig.7b. It can be seen that the presence of niobium in the supports hinders the evolution of CO. This could be related to the lower retention capacity of CO showed by the catalysts, which could be due to the presence of carbonates in the surface (as confirmedby XPS analysis of theC1sspectra) or, more likely, due to the weak CO adsorption on the support.

Temperature-programmed desorption of hydrogen was performed (Fig. 8) to characterize the thermal evolution of hydrogen chemisorbed on the $Pt/xCeO_2$-$(1-x)Nb_2O_5$catalysts. A hydrogen desorption peak at low temperature, around 400 K, can be observed, which was much more intense for catalysts with x = 0.9and x = 0.4. It is known that hydrogen desorption on ceria starts at low temperature (373 K), and it is related to the presence of dispersed noble metal [47]. Additionally, desorption peaks at slightly higher temperatures can be related to direct desorption from the metal and with a reverse spillover from the support. In this case, an overlap between the two processes is unavoidable. The presence of this peak may be interpreted as due to a change in the desorption mechanism, associated with the presence of dispersed and small platinum nanoparticles. The reverse spillover mechanism, which mainly govern the desorption process, is much faster than the direct recombination of the hydrogen species chemisorbed on the support. Another interpretation is associated with the weak capacity of the support to withhold hydrogen.

3.2. Catalytic behaviour

3.2.1. COPROX: effect of reaction temperature and reduction temperature.

The reaction profiles in terms of CO conversion and yield to CO_2 for the $Pt/xCeO_2$-$(1-x)Nb_2O_5$catalysts, at different reaction and reduction temperatures, are shown in Fig. 9 and Fig. 10, respectively (gas mixture feed: 2% CO, 2% O_2, 20% H_2 balanced in He).

The light-off curves in Fig.9 show the influence of the added cation (niobium) and on the reduction temperature in the PROX reaction.The niobia-supported catalyst shows a very low activity, with the onset of CO oxidation occurring at 673–683 K, irrespective of the reduction temperature. On the other hand, the ceria supported catalyst achieves the maximum conversion of around 85% at 390 K. The addition of niobiuminduces adecrease in the temperature at which the maximum conversion is achieved (around 353 K) and, furthermore, the maximum conversion is even increased (93-95 %). It can be also seen (Fig. 9) that a higher reduction temperature slightly increases the catalytic activity of $Pt/0.9CeO_2$-$0.1Nb_2O_5$and $Pt/0.4CeO_2$-$0.6Nb_2O_5$catalysts, but diminishes activity forcatalyst with x = 0.7. The influence of reduction temperature on activity is low for these catalysts.

At this point, it is interesting to analyze why incorporation of niobium produces an improvement in the CO conversion. As described before, XRD results showed the presence of CeO_2 and Nb_2O_5 phases in the $Pt/0.4CeO_2$-$0.6Nb_2O_5$catalyst, although the existence of a mixed oxide is also indicated. These observations are in close agreement with Raman characterization. Furthermore, TPR analysis showed that the reduction treatment at 523 K was ableto produce the surface reduction of support, and consequently, to promote the creation of oxygen vacancies. Taking into account that previous studies [48-51]have anticipated that the amount of CO adsorbed by the catalyst depends significantly on the concentration of facile lattice oxygen, the improved redox properties [Ce^{4+}/Ce^{3+}] after niobium incorporation could be responsible for the improved oxidation properties. Guerrero *et al*. [15]studied the preferential oxidation of CO and showed that niobium acted as a promoter of Pt/Al_2O_3 catalysts. The activity and yield increased for low niobium loadings on these systems, although the oxidation of CO was largely inhibited for Pt supported on pure Nb_2O_5. These authors suggest that niobia was able to weaken the CO adsorption, thus modifying the catalytic behavior in CO oxidation. CO adsorption was too weak in Pt/Nb_2O_5 and, thus, this catalyst was not active. In our case, it is interesting to notethat the PROX performanceisconsistent with the TPD results; thus, the higher CO conversion observed for the Nb-containing catalysts, at low temperature, can be related to the weaker CO adsorption. Thus, both

the lowering of the temperature of reduction of the support due to the presence of a mixed Ce-Nb oxide, and the effect of niobia on the strength of CO adsorption can explain the enhanced performance of catalysts with Nb-containing supports in CO oxidation.

The evolution of $CO_2$with temperature is very similar for all the catalysts (Fig. 10). It increases until a maxima at about 353 K for the doped catalysts and 393 K for that with the pure ceria support, and then decreases with further increase in reaction temperature, irrespective of the reduction temperature used. Furthermore, CO_2 production was not observed for the Pt/Nb_2O_5 catalyst. In all cases, catalysts with niobium-doped supportsexhibit improved CO_2 yield compared to the pure ceria-supported catalyst. The performance of the $Pt/0.7CeO_2$-$0.3Nb_2O_5$catalyst is noteworthy, with a high CO conversion (85%) and a high yield (around 0.6) after a reduction treatment at 523 K.

3.2.2. CO PROX: effect of feed composition

The influence of the feed composition on the catalytic performancehas been analyzed by varying the λ value ($\lambda = 2[O_2]/[CO]$) of the feed stream, using a feed composition of 2% CO, 0.6-2% O_2, 20 % H_2 balanced with He. Results obtained for catalyst $Pt/0.7CeO_2$-$0.3Nb_2O_5$ reduced at 523 K, and at a reaction temperature of 353 K, are shown in Fig. 11. The CO conversion depends greatly on the λ value. As can be observed, there is an increase in the catalytic activity with an increase in the O_2 content. This increase is accompanied by a decrease in the selectivity towards CO_2, whereas the oxygen conversion remains unchanged. In other words, under oxygen rich conditions both CO and H_2 oxidation are favored. These results are in agreement with previous studies[52-55], where a COoxidation dependence with λ is reported.

3.2.3. CO PROX: effect of CO_2 and H_2O in the feed.

The majority of studies on the CO preferential oxidation reaction in the presence of $H_2$are performed using gas mixtures consisting of CO, O_2, H_2 and an inert component, He or N_2[27, 28, 52, 56-60]. However, this feed does not completely simulate the actual conditions of a reforming system where, besides the mentioned gases, there is a certain amount of CO_2 and H_2O present in the feed composition.Thus, the effect of CO_2 and H_2O addition on the feed composition was studied for $Pt/0.7CeO_2$-$0.3Nb_2O_5$. The

resultsobtained, in terms of CO conversion and CO_2 yield as a function of the reaction temperature are shown in Fig. 12 for the catalyst reduced at 523 K.

The presence of CO_2in the feed stream produces a slight improvement of the catalytic activity at low reaction temperatures, but a decrease at higher temperatures. Additionally, it is possible to observe a slight decrease in the yield at high temperature. The same behavior has been observed by Ayastuy*et al.*[28]for Pt catalysts supported on $CeZrO_2$. According with these authors, the presence of CO_2 appears to affect the reaction mechanism due to modification of the distribution of the products adsorbed on platinum. In addition, at low temperatures the CO poisoning effect is clearly reduced, which may explain the slight increase in the catalytic activity. However, it has also been reported that the presence of CO_2in the feed stream inhibits CO oxidation over Pt/CeO_2 catalysts due to the formation of carbonates on the cerium oxide surfacewhich leads to a deactivation ofits redox properties[52]. As it can be seen in Fig.12b, the presence of CO_2has a greater (and beneficial) effect on hydrogen oxidation, so that the CO_2yield decreases.

Water addition to the feed streambarely affects the catalytic behavior of the studied catalyst. This may indicate that, in some way, the presence of-OH groups on the support surface promotes the catalytic activity. These results are in agreement with those obtained in the study of the reaction by DRIFTS (see below), which reflect the influence of the presence of hydroxyl groups in the catalysts surface in the CO oxidation reaction. Parinyasawan*et al.*[61]found the same tendency for $PdPt/CeO_2$ catalysts. However, Ayastuy*et al*.[28]evaluated the catalytic activity of $Pt/CeZrO_2$ and found that the presence of water had a negative effect, with a decrease at low temperatures.Moreover,the activity is hardly affected at higher temperatures.

In the case of the simultaneous presence of CO_2 and H_2O in the feed stream, a negative effect on the catalytic activity is observed, which may be attributed to competitive adsorption on the active sites. Similar results have been found for other systems. Ayastuy*et al*.[52]studied Pt/CeO_2 catalysts and found that the activity was greatly affected by the presence of both CO_2 and H_2O, and this effect showed a dependance on the reaction temperature. At low temperatures the catalytic activity decreased, but the effect was negligible at higher temperatures. Gamarra*et al*.[62]havesuggested that the negative effect of $CO_2$and H_2O in the feed is due to formation of specific carbonatesat the interfacial sitesand the blockage of active sites by adsorbed water molecules. Monyanon*et al.*[57]also found a negative effect of the

presence of CO_2 and H_2O on the activity, especially at low temperatures. This fact was closely related to the presence of carbonates and water vapor.

3.2.2. CO PROX: Operando DRIFT spectroscopy.

DRIFTS experiments have been performed in order to analyze in detail the different steps taking place in the course of the catalytic reaction. Fig. 13 shows the behavior of Pt/CeO_2 and $Pt/0.7CeO_2$-$0.3Nb_2O_5$catalysts during the PROX reaction with a feed stream containing 20 % H_2, 2 % CO, 10 % air and N_2 as balance. Prior to the experiments, the catalysts were reduced *in situ*, under flowing hydrogen, at 523 K for 1 h.

The presence of bands in theregion between 3500 and 3000 cm^{-1}, attributed to surface hydroxyl groups(-OH) and water molecules adsorbed on the support, can be observed for both catalysts. During the course of the PROX reaction, an increase in the reaction temperature for both catalyst gives rise to a decrease in the signals attributed to water and hydroxyls groups (bands at 3640, 3511, and ~ 3180 cm^{-1}), this decrease being acute in the temperature range 313-333 K. Furthermore, an increase in reaction temperature gives rise to a significant decrease in the intensity of the carbonate bands at 1567 and 1292 cm^{-1}. Furthermore, this decrease is slightly more significant for the pure ceria supported catalyst. As described in the literature[55, 63], the surface -OH groups may facilitate the formation of carbonate species by reaction with CO. Föttinger*et al.* [63]suggested that the formation of carbonates may be associated with two mechanisms, the first one being related with the dissociation of CO on the noble metal followed by the reaction of CO_2 with the support to form the surface carbonates, and the second one being related with the direct reaction between CO and -OH groups of the support, followed by CO_2 reaction with additional -OH groups. Shido*et al.* [64]studied Rh/CeO_2 in the WGS reaction and observed the formation of bidentateformates from CO and surface -OH groups on ceria. Daté*et al.* [65]studied the influence of humidity on the CO oxidation reaction on gold catalysts prepared on different supports. According to these authors, the reaction mechanism depends on the nature of the support and on the presence of moisture; moisture improves the reaction activity due to the involvement of -OH group as intermediates. Xu *et al.* [66]also studied the reaction mechanism of WGS and PROX reactions. In this case, CO_2 formation occurred through the reaction between adsorbed CO and surface -OH groups (CO_{ads} + OH_{surf}) taking place at Pt-oxide interface

sites at low temperature. Graf *et al.* [67]determined that the reactivity of hydroxyl groups on Pt catalysts for the WGS reaction is associated with the formate formation by mono-coordinated hydroxyls. Taking into account this reports, probably one reaction mechanism could be that the CO can react with -OH surface groups of the support to form carbonates and formates until total saturation; then, the reaction could move towards Pt surface sites, leading to a lesser, but constant activity.

Peaks at 2032 and 2055 cm^{-1} can be assigned to linearly adsorbed CO on a single Pt metal for Pt/CeO_2 and $Pt/0.7CeO_2$-$0.3Nb_2O_5$ catalysts, respectively.[48, 55, 67, 68]. The difference between both catalysts suggests a different morphology of Pt nanoparticles depending on the support used and/or on the relative surface coverage of CO and oxygen under analogous conditions. It is known that the υ (CO) frequency is sensitive to the platinum coordination, and it shifts to lower frequencies when the coordination decreases. Furthermore, small metal particles possess low Pt coordination and CO adsorption on these sites is characterized by lower wavenumbers[67, 68]. The presence of this band at lower wavenumbers in the pure ceria catalyst could be associated to the presence of small nanoparticles together with the presence of defect sites at the metal-support interface which are able to tilt CO adsorption [69]. On the contrary, the peak at 2055 cm^{-1} in the niobium-ceria supported catalyst could be associated to the presence of more coordinated Pt atoms.

Interestingly, the Pt/CeO_2 catalyst exhibits a decrease in the characteristic bands of bidentate carbonates at 1567 and 1292 cm^{-1}, and an increase of unidentate carbonates at 1547 cm^{-1}. However, in the case of $Pt/0.7CeO_2$-$0.3Nb_2O_5$, a decrease of bidentate carbonate bands and an increase of formate band at 1364 cm^{-1} is observed[55, 70-75]. These results suggest that both the oxide surface and the morphology of the Pt nanoparticles depend significantly on the nature of the oxide support, i.e., to the presence or absence of niobium, and that this affects the catalytic activity.

4. Conclusions

A series of Pt/CeO_2-Nb_2O_5 catalysts were prepared using different proportions of cerium and niobium in the support, and studied in the preferential oxidation of CO in the presence of hydrogen. By using different characterization techniques it has been possible to determine that the formation of a true mixed oxide is formed, although there is a high surface segregation of Nb, as determined by XPS. CO-TPD experiments showed that the presence of Nb in the supports decreased the catalysts' ability to adsorb

CO.Despite the fact thatthe Pt/Nb_2O_5 catalyst was almost inactive in the PROX reaction, higher catalytic activities, especially at lower temperatures, were obtained with catalysts based onniobia-ceria supports. The best catalytic performance was obtained with the $Pt/0.7CeO_2$-$0.3Nb_2O_5$catalyst, which achieved a high CO conversion (85%) and a high yield (around 0.6) after a reduction treatment at 523 K.

Acknowledgments

The authors gratefully acknowledge the financial support from the MINECO (Spain, Project MAT2010-21147)and GeneralitatValenciana (PROMETEO/2009/002 – FEDER and PROMETEOII/2014/004 – FEDER). EVRF thanks the MINECO for his Ramón y CajalFellowship. EOJ thanks the CNPq– Brazil for her grant.We thank Drs S.B. Campbell and F.M. McKenna, University of Aberdeen for assistance in performing the DRIFT experiments.

References

[1] A. Trovarelli, 2002)

[2] X. Wang, R.J. Gorte, J.P. Wagner, J. Catal. 212 (2002) 225-230.

[3] E. Mamontov, T. Egami, R. Brezny, M. Koranne, S. Tyagi, The Journal of Physical Chemistry B 104 (2000) 11110-11116.

[4] K. Eguchi, T. Setoguchi, T. Inoue, H. Arai, Solid State Ionics 52 (1992) 165-172.

[5] H. Hayashi, R. Sagawa, H. Inaba, K. Kawamura, Solid State Ionics 131 (2000) 281-290.

[6] M. O´Connell, M.A. Morris, Catal. Today 59 (2000) 387-393.

[7] E. Ramírez-Cabrera, A. Atkinson, D. Chadwick, Appl. Catal. B: Environ. 36 (2002) 193-206.

[8] M. Casapu, A. Bernhard, D. Peitz, M. Mehring, M. Elsener, O. Kröcher, Appl. Catal. B: Environ. 103 (2011) 79-84.

[9] E. Ramírez-Cabrera, A. Atkinson, D. Chadwick, Solid State Ionics 136–137 (2000) 825-831.

[10] A. Aronne, M. Turco, G. Bagnasco, G. Ramis, E. Santacesaria, M. Di Serio, E. Marenna, M. Bevilacqua, C. Cammarano, E. Fanelli, Appl. Catal. A. : Gen. 347 (2008) 179-185.

[11] N. Laosiripojana, W. Sutthisripok, P. Kim-Lohsoontorn, S. Assabumrungrat, Int. J. Hydrogen Energy 35 (2010) 6747-6756.

[12] K. Yashiro, T. Suzuki, A. Kaimai, H. Matsumoto, Y. Nigara, T. Kawada, J. Mizusaki, J. Sfeir, J. Van herle, Solid State Ionics 175 (2004) 341-344.

[13] I.K. Naik, T.Y. Tien, J. Electrochem. Soc. 126 (1979) 562-566.

[14] M.R. De Guire, M.J. Shingler, E. Dincer, Solid State Ionics 52 (1992) 155-163.

[15] S. Guerrero, J.T. Miller, E.E. Wolf, Appl. Catal. A. : Gen. 328 (2007) 27-34.

[16] P. Marques, N.F.P. Ribeiro, M. Schmal, D.A.G. Aranda, M.M.V.M. Souza, J. Power Sources 158 (2006) 504-508.

[17] D. Stosic, S. Bennici, V. Rakic, A. Auroux, Catal. Today 192 (2012) 160-168.

[18] M. Thammachart, V. Meeyoo, T. Risksomboon, S. Osuwan, Catal. Today 68 (2001) 53-61.

[19] M. Paulis, M. Martín, D.B. Soria, A. Díaz, J.A. Odriozola, M. Montes, Appl. Catal. A. : Gen. 180 (1999) 411-420.

[20] R. Brayner, D. Ciuparu, G.M. da Cruz, F. Fiévet-Vincent, F. Bozon-Verduraz, Catalysis Today 57 (2000) 261-266.

[21] S. Zhao, R.J. Gorte, Appl. Catal. A. : Gen. 248 (2003) 9-18.

[22] J.M. Jehng, I.E. Wachs, Chemistry of Materials 3 (1991) 100-107.

[23] R.J. Cava, R.S. Roth, T. Negas, H.S. Parker, D.B. Minor, J. Solid State Chem. 40 (1981) 318-329.

[24] B.M. Reddy, A. Khan, Y. Yamada, T. Kobayashi, S. Loridant, J.C. Volta, The Journal of Physical Chemistry B 107 (2003) 11475-11484.

[25] Q. Wu, J. Chen, J. Zhang, Fuel Process. Technol. 89 (2008) 993-999.

[26] S. Kundu, J. Ciston, S.D. Senanayake, D.A. Arena, E. Fujita, D. Stacchiola, L. Barrio, R.M. Navarro, J.L.G. Fierro, J.A. Rodriguez, The Journal of Physical Chemistry C 116 (2012) 14062-14070.

[27] G. Avgouropoulos, M. Manzoli, F. Boccuzzi, T. Tabakova, J. Papavasiliou, T. Ioannides, V. Idakiev, J. Catal. 256 (2008) 237-247.

[28] J.L. Ayastuy, M.P. González-Marcos, A. Gil-Rodríguez, J.R. González-Velasco, M.A. Gutiérrez-Ortiz, Catal. Today 116 (2006) 391-399.

[29] P. Fornasiero, G. Balducci, R. Di Monte, J. Kaspar, V. Sergo, G. Gubitosa, A. Ferrero, M. Graziani, Journal of Catalysis 164 (1996) 173-183.

[30] A. Martínez-Arias, D. Gamarra, M. Fernández-García, X.Q. Wang, J.C. Hanson, J.A. Rodríguez, J. Catal. 240 (2006) 1-7.

[31] S. Ricote, G. Jacobs, M. Milling, Y. Ji, P.M. Patterson, B.H. Davis, Appl. Catal. A. : Gen. 303 (2006) 35-47.

[32] R. Buitrago, J. Ruiz-Martínez, J. Silvestre-Albero, A. Sepúveda-Escribano, F. Rodríguez-Reinoso, Catal. Today 180 (2012) 19-24.

[33] J. Silvestre-Albero, F. Rodríguez-Reinoso, A. Sepúlveda-Escribano, J. Catal. 210 (2002) 127-136.

[34] J. Silvestre-Albero, F. Coloma, A. Sepúlveda-Escribano, F. Rodríguez-Reinoso, Appl. Catal. A. : Gen. 304 (2006) 159-167.

[35] A.F. Carley, M.W. Roberts, A.K. Santra, The Journal of Physical Chemistry B 101 (1997) 9978-9983.

[36] J.L.G. Fierro, L.G. Tejuca, Appl. Surf. Sci. 27 (1987) 453-457.

[37] G.U. Kulkarni, C.N.R. Rao, M.W. Roberts, The Journal of Physical Chemistry 99 (1995) 3310-3316.

[38] N. Yamazoe, Y. Teraoka, T. Seiyama, Chem. Lett. 10 (1981) 1767-1770.

[39] L. Richter, S.D. Bader, M.B. Brodsky, Physical Review B 22 (1980) 3059-3064.

[40] J.L.G. Fierro, Catal. Today 8 (1990) 153-174.

[41] T.H. Fleisch, R.F. Hicks, A.T. Bell, J. Catal. 87 (1984) 398-413.

[42] L. González Tejuca, A.T. Bell, J.L.G. Fierro, M.A. Peña, Appl. Surf. Sci. 31 (1988) 301-316.

[43] K. Musialska, E. Finocchio, I. Sobczak, G. Busca, R. Wojcieszak, E. Gaigneaux, M. Ziolek, Appl. Catal. A. : Gen. 384 (2010) 70-77.

[44] E.V. Ramos-Fernandez, N.R. Shiju, G. Rothenberg, RSC Advances 4 (2014) 16456-16463.

[45] I. Atribak, A. Bueno-López, A. García-García, J. Mol. Catal. A: Chem. 300 (2009) 103-110.

[46] Z. Zhang, X. Du, W. Wendong, J. Vac. Sci. Technol. , A 18 (2000) 2928-2931.

[47] S. Bernal, J.J. Calvino, M.A. Cauqui, J.M. Gatica, C. Larese, J.A. Pérez Omil, J.M. Pintado, Catal. Today 50 (1999) 175-206.

[48] R. Craciun, B. Nentwick, K. Hadjiivanov, H. Knözinger, Appl. Catal. A. : Gen. 243 (2003) 67-79.

[49] F. Dong, T. Tanabe, A. Suda, N. Takahashi, H. Sobukawa, H. Shinjoh, Chem. Eng. Sci. 63 (2008) 5020-5027.

[50] L.M. Molina, B. Hammer, Physical Review B 69 (2004) 155424-

[51] K. Ramesh, L. Chen, F. Chen, Y. Liu, Z. Wang, Y.F. Han, Catal. Today 131 (2008) 477-482.

[52] J.L. Ayastuy, A. Gil-Rodríguez, M.P. González-Marcos, M.A. Gutiérrez-Ortiz, Int. J. Hydrogen Energy 31 (2006) 2231-2242.

[53] F. Mariño, C. Descorme, D. Duprez, Appl. Catal. B: Environ. 54 (2004) 59-66.

[54] F. Mariño, C. Descorme, D. Duprez, Appl. Catal. B: Environ. 58 (2005) 175-183.

[55] O. Pozdnyakova, D. Teschner, A. Wootsch, J. Kröhnert, B. Steinhauer, H. Sauer, L. Toth, F.C. Jentoft, A. Knop-Gericke, Z. Paál, R. Schlögl, J. Catal. 237 (2006) 1-16.

[56] O.H. Laguna, E.M. Ngassa, S. Oraá, A. Álvarez, M.I. Domínguez, F. Romero-Sarria, G. Arzamendi, L.M. Gandía, M.A. Centeno, J.A. Odriozola, Catal. Today 180 (2012) 105-110.

[57] S. Monyanon, S. Pongstabodee, A. Luengnaruemitchai, J. Power Sources 163 (2006) 547-554.

[58] E. Moretti, M. Lenarda, L. Storaro, A. Talon, T. Montanari, G. Busca, E. Rodríguez-Castellón, A. Jiménez-López, M. Turco, G. Bagnasco, R. Frattini, Appl. Catal. A. : Gen. 335 (2008) 46-55.

[59] M.M. Schubert, A. Venugopal, M.J. Kahlich, V. Plzak, R.J. Behm, J. Catal. 222 (2004) 32-40.

[60] H. Zou, S. Chen, Z. Liu, W. Lin, Int. J. Hydrogen Energy 34 (2009) 9324-9333.

[61] A. Parinyaswan, S. Pongstabodee, A. Luengnaruemitchai, Int. J. Hydrogen Energy 31 (2006) 1942-1949.

[62] D. Gamarra, A. Marí¡nez-Arias, J. Catal. 263 (2009) 189-195.

[63] K. Föttinger, R. Schlogl, G. Rupprechter, Chemical Communications 2008) 320-322.

[64] T. Shido, Y. Iwasawa, J. Catal. 141 (1993) 71-81.

[65] M. Daté, M. Okumura, S. Tsubota, M. Haruta, Angew. Chem. , Int. Ed. 43 (2004) 2129-2132.

[66] L. Xu, Y. Ma, Y. Zhang, Z. Jiang, W. Huang, J. Amer. Chem. Soc. 131 (2009) 16366-16367.

[67] P.O. Graf, D.J.M. de Vlieger, B.L. Mojet, L. Lefferts, J. Catal. 262 (2009) 181-187.

[68] M. Shen, L. Lv, J. Wang, J. Zhu, Y. Huang, J. Wang, Chem. Eng. J 255 (2014) 40-48.

[69] F. Coloma, J. Coronado, C. Rochester, J. Anderson, Catalysis Letters 51 (1998) 155-162.

[70] A. Badri, C. Binet, J.C. Lavalley, The Journal of Physical Chemistry 100 (1996) 8363-8368.

[71] P. Bera, A. Hornés, A.L. Cámara, A. Martínez-Arias, Catal. Today 155 (2010) 184-191.

[72] C. Binet, M. Daturi, J.C. Lavalley, Catal. Today 50 (1999) 207-225.

[73] K. Fottinger, R. Schlogl, G. Rupprechter, Chem. Commun. 2008) 320-322.

[74] A. Martínez-Arias, A.B. Hungría, M. Fernández-García, J.C. Conesa, G. Munuera, J. Power Sources 151 (2005) 32-42.
[75] D. Teschner, A. Wootsch, O. Pozdnyakova-Tellinger, J. Kröhnert, E.M. Vass, M. Hävecker, S. Zafeiratos, P. Schnörch, P.C. Jentoft, A. Knop-Gericke, R. Schlögl, J. Catal. 249 (2007) 318-327.

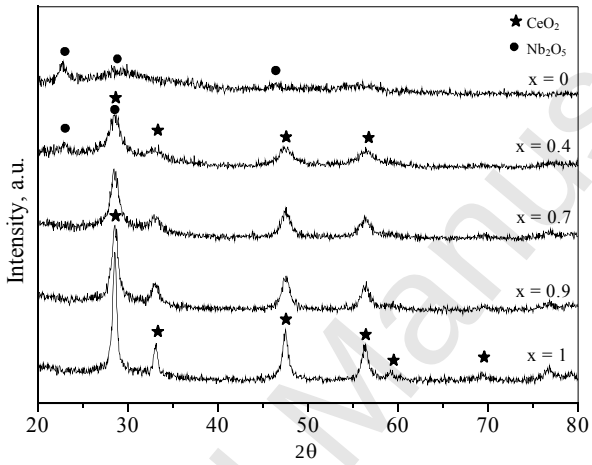

Fig. 1. XRD patterns of $Pt/xCeO_2$-$(1-x)Nb_2O_5$ catalysts, with x = 1, 0.9, 0.7, 0.4 and 0.

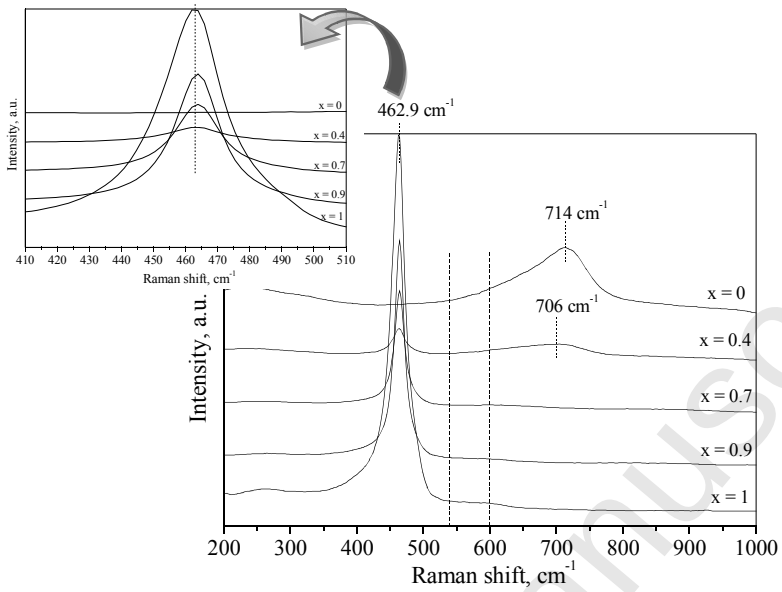

Fig. 2. Raman spectra of $xCeO_2$-$(1-x)Nb_2O_5$, with x = 0, 0.4, 0.7, 0.9 and 1.

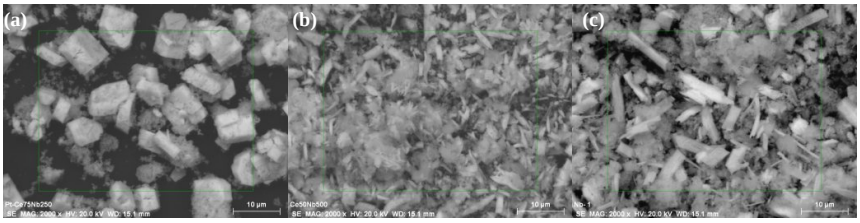

Fig. 3a. SEM images for (a) Pt/0.9CeO_2-0.1Nb_2O_5, (b) Pt/0.7CeO_2-0.3Nb_2O_5 and (c) Pt/0.4CeO_2-0.6Nb_2O_5.

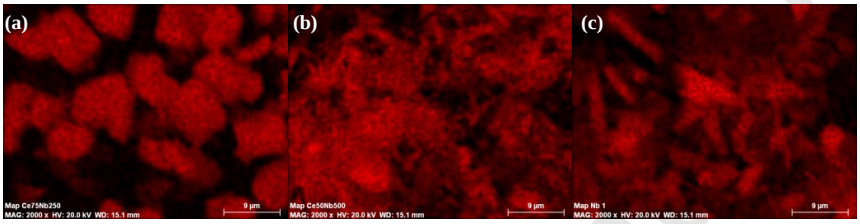

Fig. 3b. SEM-chemical mapping Ce analysis (red), for (a) Pt/0.9CeO_2-0.1Nb_2O_5, (b) Pt/0.7CeO_2-0.3Nb_2O_5 and (c) Pt/0.4CeO_2-0.6Nb_2O_5.

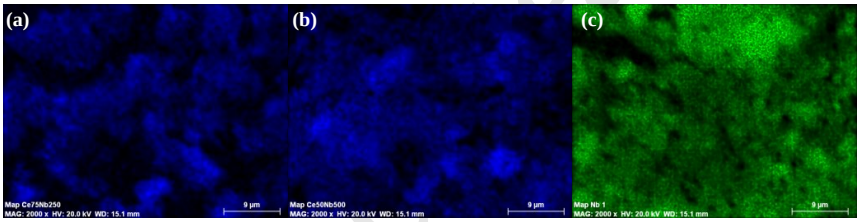

Fig. 3c. SEM-chemical mapping Nb analysis (blue and green) for (a) Pt/0.9CeO_2-0.1Nb_2O_5, (b) Pt/0.7CeO_2-0.3Nb_2O_5 and (c) Pt/0.4CeO_2-0.6Nb_2O_5.

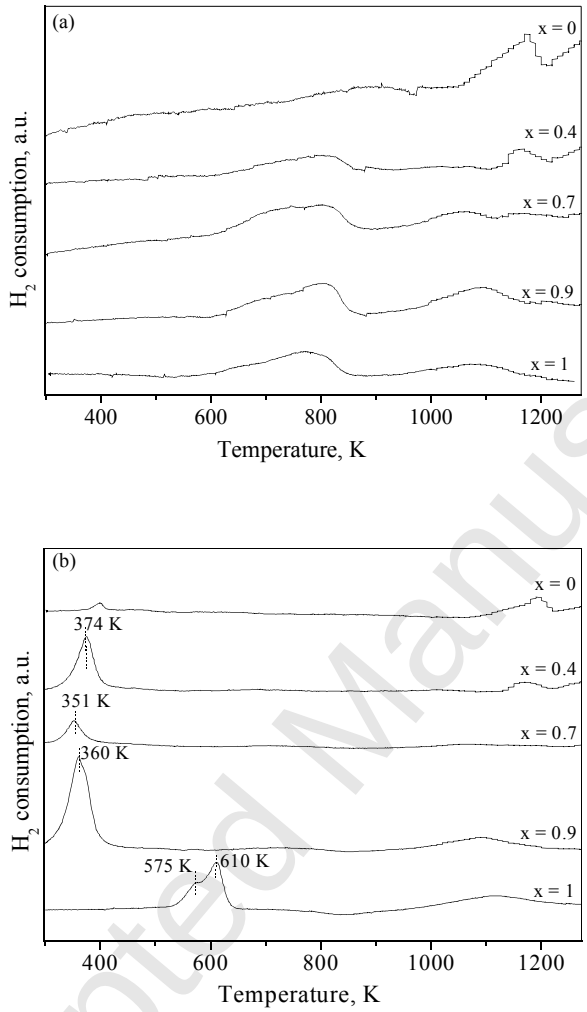

Fig. 4. TPR profiles of (a) $xCeO_2$-(1-x)Nb_2O_5 and (b) Pt/$xCeO_2$-(1-x)Nb_2O_5 (b), with x = 1, 0.9, 0.7, 0.4 and 0.

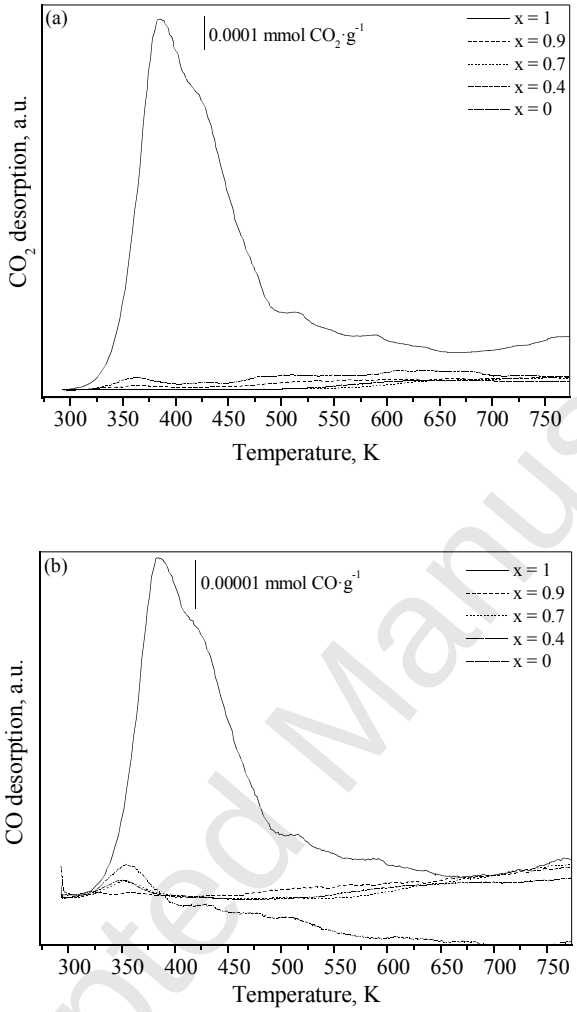

Fig. 5. (a) CO_2 and (b) CO desorption profiles for $Pt/xCeO_2$-$(1-x)Nb_2O_5$ catalysts reduced at 523 K, with x = 1, 0.9, 0.7, 0.4 and 0.

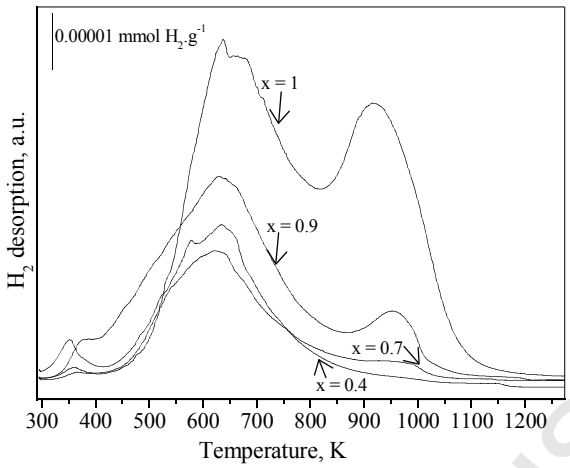

Fig. 6. H_2 desorption profiles for $Pt/xCeO_2$-$(1-x)Nb_2O_5$ catalysts reduced at 523 K.

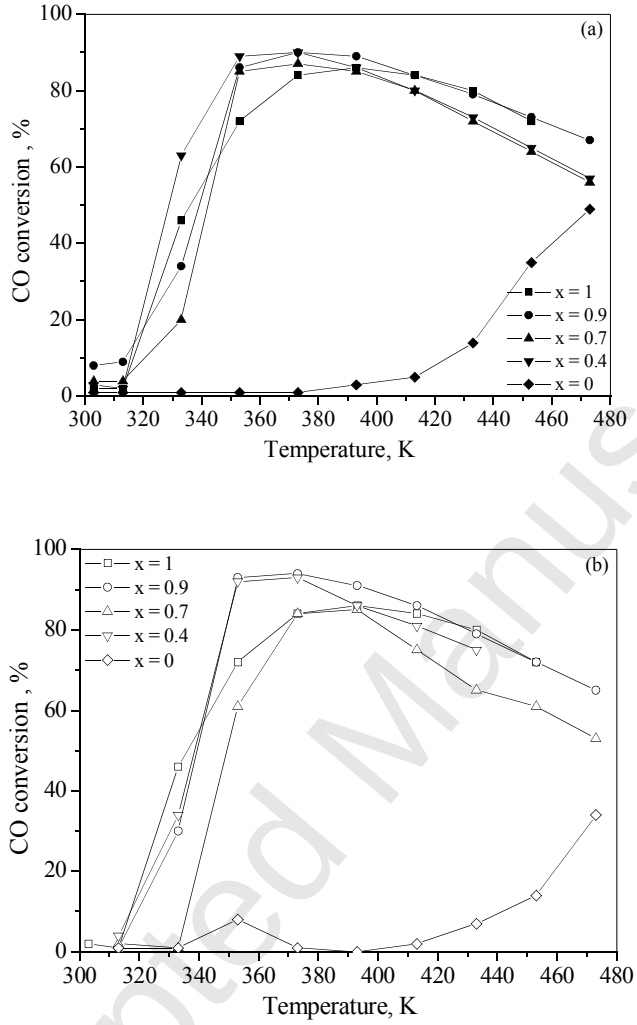

Fig. 7. CO oxidation light-off curves for Pt/xCeO_2-(1-x)Nb_2O_5 series catalysts, reduced at (a) 523 K and (b), 773 K gas mixture feed: 2% CO, 2% O_2, 20% H_2 balanced in He.

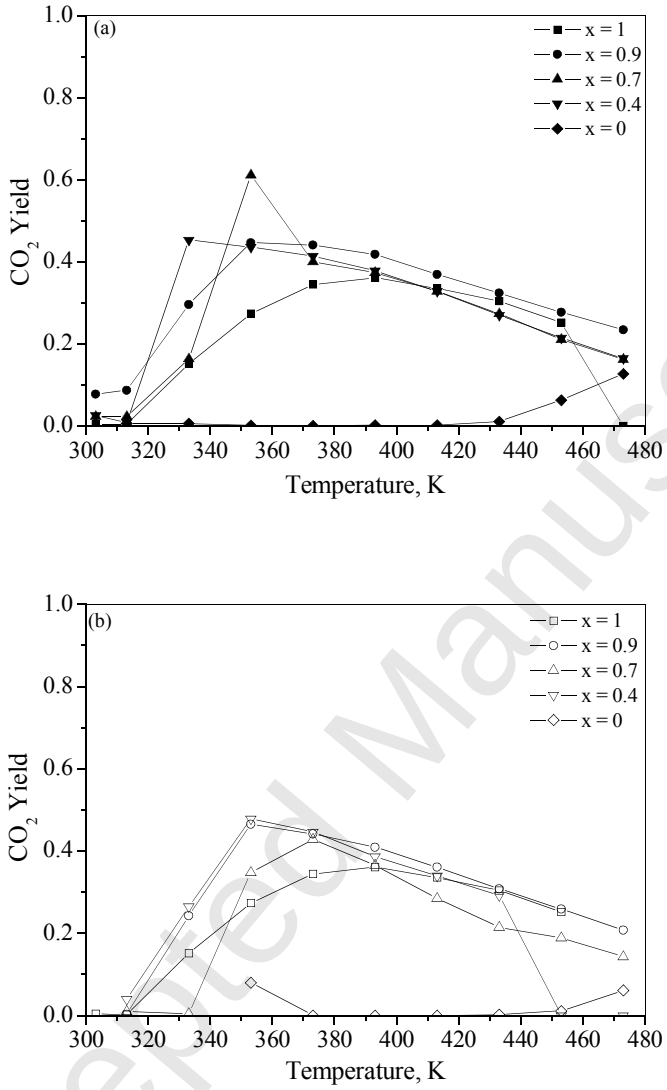

Fig. 8. CO_2 yields for Pt/xCeO_2-(1-x)Nb_2O_5 series catalysts, reduced at (a) 523 K and (b), 773 K gas mixture feed: 2% CO, 2% O_2, 20% H_2 balanced in He.

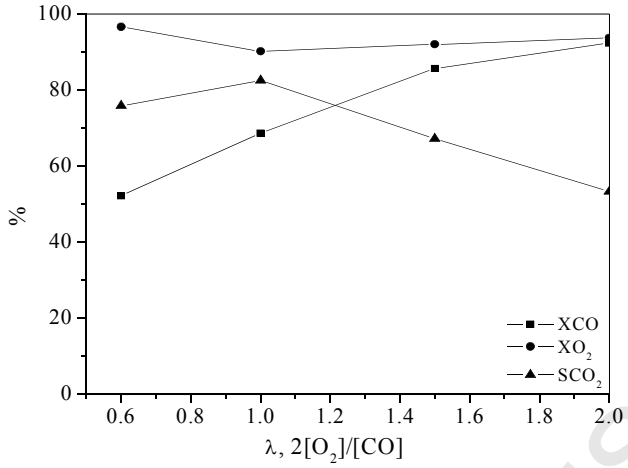

Fig. 9. CO preferential oxidation over Pt/0.7CeO_2-0.3Nb_2O_5 catalyst, reduced at 523 K and with the reaction temperature at 353 K, in a feed of 2% CO, 0.6-2% O_2, 20% H_2 and He as balance.

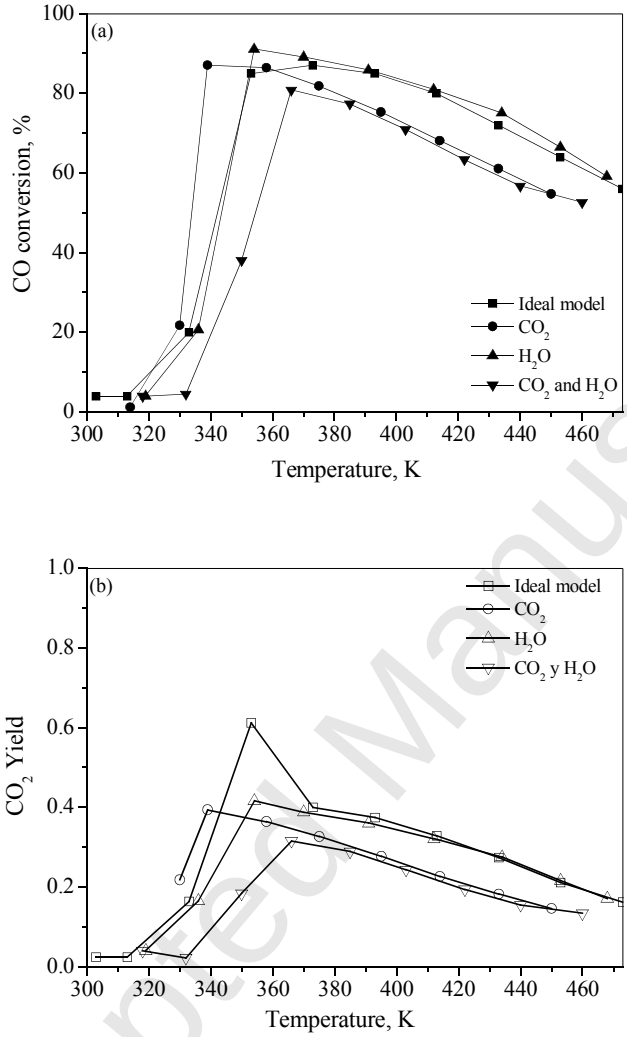

Fig. 10. CO conversion (a) and CO_2 yield (b) under different feed conditions (2% CO, 2% O_2, 20% H_2, 0-5% CO_2, 0-5 % H_2O and He as balance) for the $Pt/0.7CeO_2$-$0.3Nb_2O_5$ catalyst.

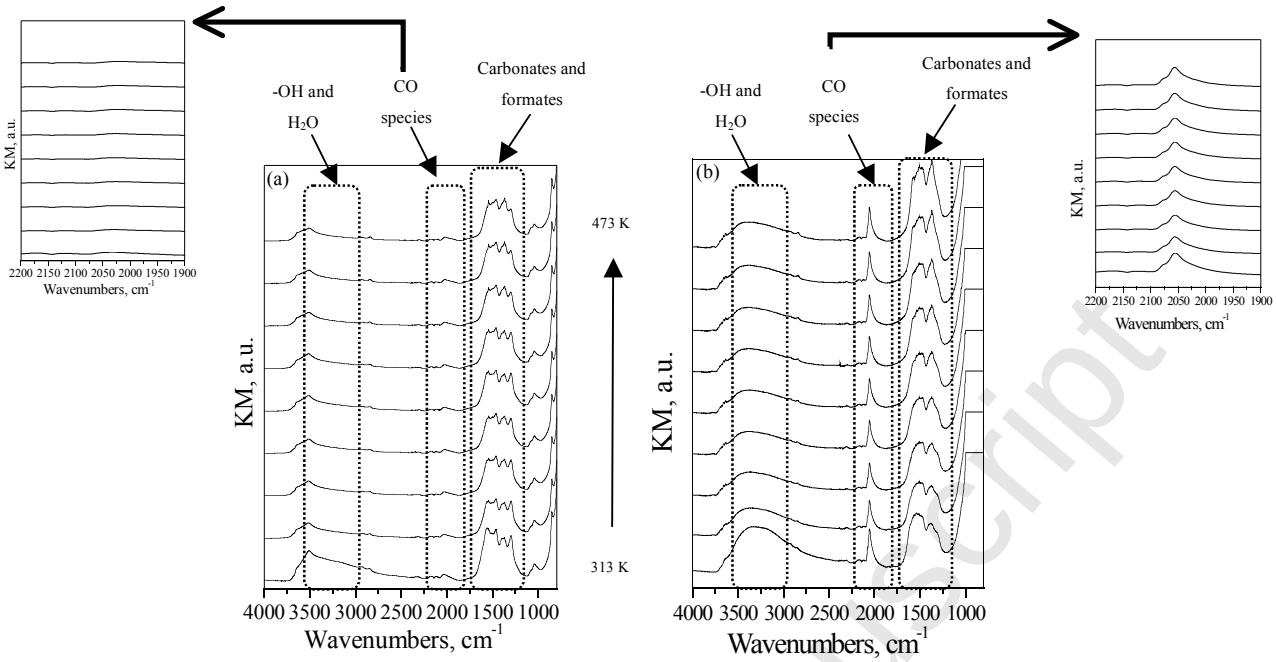

Fig. 11. DRIFT spectra obtained during CO oxidation in 2% CO, 10% air, 20% H_2 and N_2 as balance feed, for Pt/CeO_2(a) and Pt/0.7CeO_2-0.3Nb_2O_5(b) previously reduced at 523 K, The initial temperature was of 313 K and increase by 20 K from bottom to top.

Table 1. Chemical composition and textural and crystallographic characterization of $Pt/xCeO_2$-$(1-x)Nb_2O_5$ catalysts.

Catalyst	Pt, wt.%	CeO_2, wt.%	Nb_2O_5,wt.%	S_{BET}, $m^2 \cdot g^{-1}$	Crystallite size, nm [(a)]	Lattice constant, nm[(a)]
x = 1	1.0	100	0	70	17	0.542
x = 0.9	0.8	89	11	90	10	0.542
x = 0.7	0.8	72	28	111	8	0.542
x = 0.4	0.8	45	55	117	6	0.542
x = 0	0.6	0	100	132	--	--

(a) Support.

Table 2. XPS characterization of $Pt/xCeO_2$-$(1-x)Nb_2O_5$ catalysts.

Catalyst	BE O 1s, eV	BE O 1s, eV	BE O 1s, eV	Nb/Ce (XPS) atomic ratio	Nb/Ce (bulk) atomic ratio
x = 1	528.9	530.7	532	0	0
x = 0.9	529.4	531	532.5	0.8	0.11
x = 0.7	529.5	531	532.5	2.3	0.32
x = 0.4	531.5	532.8	534.3	3	1.01
x = 0	530.6	532	533.3	--	--

*Graphical Abstract (for review)